Modeling and optimization of laser shock hole-clinching using response surface methodology and genetic algorithm

Haoyu Yuan[1] · Changdong Pan[2] · Libin Song[3] · Guoqun Zhao[3] · Chao Zheng[3]

Abstract
Laser shock hole-clinching is one of mechanical joining processes in which metal foils are joined together based on plastic deformation caused by laser-induced shock wave. In the process, fracture often occurs due to the unreasonable arrangement of laser process parameters, suggesting that it is urgent to seek a feasible way to improve the joint forming quality. However, it consumes a great deal of time and effort to obtain the optimal solution of process parameters from so many different combinations through experiments and numerical simulations. In this study, the mathematical models between laser process parameters and joint forming quality were established through response surface methodology (RSM). A finite element analysis model of laser shock hole-clinching process for pure copper and pre-pierced stainless steel foils was developed, and then it was used to perform the calculation scheme arranged by design of experiments. Analysis of variance (ANOVA) was implemented to evaluate the statistical significance of RSM models and the influence of process parameters on objectives. Multi-objective optimization was carried out to achieve the optimal combination of laser process parameters by using genetic algorithm (GA). It is revealed that the RSM-GA-integrated approach is an effective way to realize the modeling and optimization of laser process parameters for laser shock hole-clinching. The pulsed laser energy (E), number of laser pulses (N), and laser spot diameter (D) are statistically significant, and both the interlock value and the maximum thinning rate are sensitive to these parameters based on ANOVA. The fitting precision analysis indicates that the established RSM models can be used to navigate the design space of variables and predict the actual data with high accuracy. Moreover, it is found that the influence order of laser process parameters on the interlock value from strong to weak is N, E, and D, while this order changes to D, N, and E for the maximum thinning rate. According to the Pareto noninferior solutions and the corresponding values of satisfaction function, the optimal combination is $E = 164$ mJ, $N = 25$, and $D = 2.1$ mm in the given design space. The GA optimization result has been experimentally confirmed.

Keywords Laser shock forming · Laser shock clinching · Optimization · Finite element analysis

1 Introduction

Laser shock hole-clinching is one of novel mechanical joining processes, in which two or more metal foils are connected together to form an interlock structure based on plastic deformation. The process derives from laser shock forming and expands this forming method to the clinching field. Therefore, no heat source or extra rivet is required, and the formation of the joint depends entirely on the cold plastic forming of joining partners. Due to the significant technological advantages, such as non-contact, flexibility, high efficiency, and lightweight, the process is eminently suitable for the demand of joining dissimilar materials with distinct differences in physical and mechanical properties, especially for metal foils with the thickness in the micron range.

The joining mechanism of laser shock hole-clinching is illustrated in Fig. 1a. Unlike a rigid punch available in conventional clinching, a laser beam with adjustable spot size is used as a soft punch. In order to provide enough laser energy to form a plasma, the laser system with ns pulse

✉ Chao Zheng
  zhengchao@sdu.edu.cn

[1] School of Mechanical Engineering, Shandong University, Jinan 250061, People's Republic of China

[2] Hyundai Motor R&D Center, Yantai 264000, People's Republic of China

[3] Key Laboratory for Liquid-Solid Structural Evolution and Processing of Materials (Ministry of Education), School of Materials Science and Engineering, Shandong University, Jinan 250061, People's Republic of China
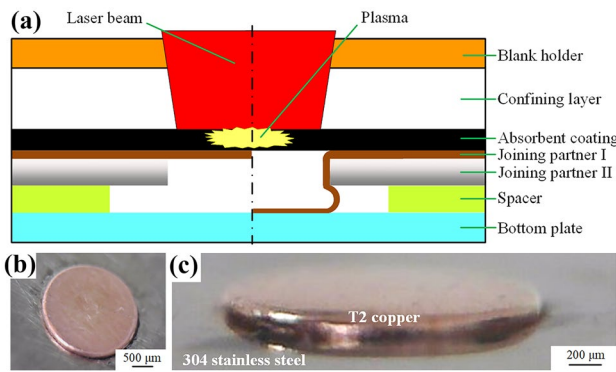
Fig. 1 **a** Schematic of laser shock hole-clinching process; **b** and **c** a typical clinched joint (T2 pure copper/304 stainless steel foils) [3]

duration, mm spot size, and the laser power density higher than 10^{12} W/m^2 level is preferred [1]. While the incident laser beam reaches the upper surface of absorbent coating, the coating immediately absorbs the laser energy in a quite short time and then forms a plasma. Owing to the confinement of confining layer, the plasma expands rapidly in a confined space, resulting in the formation of a shock wave. The shock wave then propagates into the joining partner I, and plastic deformation is caused, while the amplitude of shock wave pressure exceeds the yield strength of the partner I. Under the continuous effect of laser-induced shock wave, the joining partner I gradually bulges into the pre-pierced hole on the joining partner II, and at last the partners are joined together by means of a form-fit joint [2]. Figure 1b, c present the morphology of a typical clinched joint with the combination of T2 pure copper and 304 stainless steel foils.

In order to realize the effective clinching of metal foils through laser-induced shock wave, the innovative design of experimental facility has attracted much more attention. Veenaas et al. [4] presented the basic realization method of laser shock hole-clinching process for dissimilar metal foils. In their experimental apparatus, there are some essential components, including the laser system, blank holder, joining partners, spacer, and bottom plate. A circular hole is pre-fabricated using laser cutting process on the lower metal foil (named the joining partner II) to enable the material from the upper metal foil (named the joining partner I) to flow into. A spacer is placed between the joining partners and the bottom plate to accommodate the inflowing material, which is crucial for the formation of interlock structure. A round-point joint with the combination of aluminum/steel is obtained after a total number of 50 pulses have been applied. Based on the principle of laser shock hole-clinching process, other clinching methods have been proposed via numerous experimental attempts, including the compound clinching without the pre-fabrication of hole [5], micro-shear clinching process [6], and incremental clinching process

[7]. However, it is noted that tens to hundreds of pulses are needed to implement laser shock experiments, which consumes a great deal of time and effort. In addition, both the adjustment of process parameters and the measurement of joint dimensions are troublesome, and thus they limit the in-depth investigation on the mechanical joining behavior of metal foils under laser shock [8].

Finite element analysis (FEA) is one of useful approaches to explore the plastic deformation behavior and to predict the forming quality in both laser shock forming and clinching processes, especially in the case that the experimental study is difficult to conduct, for example, the material flowing characteristics, the strain/stress distribution, and the evolution of interlock structure [9]. Wang et al. [10] employed LS-DYNA software to analyze the deformation history of clinched joint, which is unable to observe through the experiment due to the enclosed die structure. The influence of laser energy and spacer height on the interlock formation is revealed with the aid of FEA results. Furthermore, Wang et al. [3] verified the feasibility to join three dissimilar metal foils in laser shock hole-clinching by FEA. After that, they carried out experiments to successfully obtain the joint with three partners by using the clinching parameters achieved from FEA. In the work proposed by You et al. [11], the application of laser shock hole-clinching was extended from a round-point joint to a linear interlock structure. In this process, the overlapping rate of laser spot plays an important role in the interlock formation, and thus its effect has been in-detailed discussed by FEA performed using ABAQUS. In our previous work [7, 10], the authors presented a FEA study on the material flowing and clinching behavior of dissimilar metal foils under multiple laser pulses. Both the temperature rise and shock wave propagation characteristics were evaluated based on the validated FEA model. The effect of laser power density on interlock value and thickness distribution was discussed by a series of simulations. Although FEA offers convenience for the research of forming and clinching processes, it still needs much time and energy to establish a numerical model with high precision and to adjust the model, while the process conditions have been changed. In addition, the application ability of FEA strongly relates to the professional knowledge of operators as well as the proficiency in FEA software.

Due to the high cost of the experimental study and the operation difficulty in FEA for analyzing the deformation behavior in metal forming and joining processes, the surrogate model method has attracted extensive attention. The main advantage of surrogate model method is that it does not require knowledge about the specialized field. In addition, the relationship between the input variables and output objectives can be determined through a specific form of surrogate function. Artificial neural network (ANN) and response surface methodology (RSM) are two of the most

frequently used surrogate models, and they are generally adopted to approximate experimental and FEA results. Lambiase and Di Ilio [12] applied ANN to the prediction of clinching behavior under different clinching tools configurations instead of the heavy finite element simulations. The predictions from the established ANN model exhibit good agreement with those from FEA and can be used for the next optimization. In laser shock peening process, ANN was used to predict the residual stress [13, 14] and mechanical properties of treated specimens [15]. Compared with ANN, an explicit function can be obtained through RSM, which is quite convenient for practical application. Davidson et al. [16] employed RSM to develop the prediction model of the surface roughness for flow-forming process. The result of the validated experiment shows that the error between the practical and predicated surface roughness is less than 6%. In order to predict the maximum temperature in incremental sheet forming, Bagudanch et al. carried out design of experiments to establish RSM model between material temperature and process parameters for different polymers [17]. The analysis of variance indicates that the proposed models are significant. Mostafanezhad et al. [18] analyzed the formability of Al alloy in two-point incremental forming process based on RSM, and analysis of variances was performed to identify the contribution of factors on the responses. The above-mentioned researches give a constructive application of surrogate model method in metal forming and clinching fields. It is noted that a large quantity of experiments and FEA can be omitted which significantly reduces the research cost, whereas the effectiveness of surrogate model method in laser shock hole-clinching process is still not assessed.

In laser shock hole-clinching process, fracture is the main forming defect, and some typical examples in our experiment are presented in Fig. 2. Therefore, it is quite necessary to reasonably arrange the process parameters, such as laser energy, spot diameter, number of pulses, and overlapping rate. However, it is not an easy task to obtain the reasonable arrangement of process parameters from so many combinations through experiments and numerical simulations, especially in the case that there are multiple targets. As a consequence, the application of optimization technologies offers a powerful way which easily deals with the requirement for the optimal combination of several variables with multiple outputs. In the field of mechanical clinching and laser shock peening processes, some optimization technologies have been successfully applied, such as design of experiments [19], Grey relational analysis [20], Kriging model [21], RSM [22], and genetic algorithm (GA) [12, 23, 24]. Among these attempts, GA is easily understood and can be conveniently implemented using MATLAB toolbox, and particularly it is powerful enough to obtain a global target for multi-objective optimization.
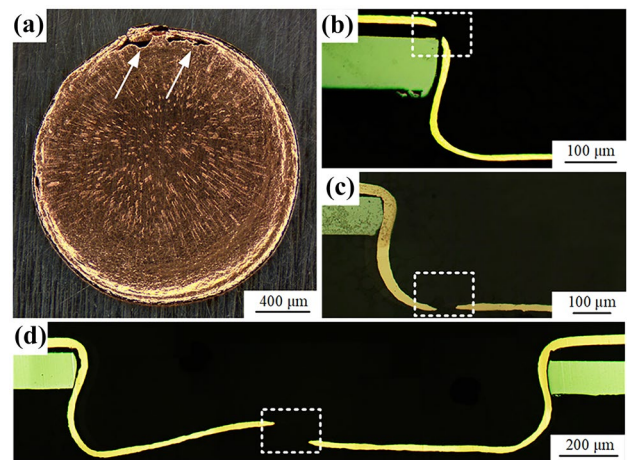

Fig. 2 Morphology of the fractured joint. **a** Global view of a typical fractured joint; **b** fracture on the neck; **c** fracture near the bottom corner; **d** fracture on the bottom surface

However, the optimal strategy of process parameters in laser shock hole-clinching is still not developed. In the light of the described challenges, it is urgent to establish an effective surrogate model and propose an optimal strategy for laser shock hole-clinching process through a detailed investigation.

The aim of the current work is to build a surrogate model which can successfully predict the forming quality indexes of clinched joint and to establish a multi-objective optimization strategy to improve the joint quality. A FEA model of laser shock hole-clinching process for pure copper and pre-pierced stainless steel foils was developed by using ABAQUS software. Central composite design (CCD) was used to arrange the FEA scheme. The second-order mathematical models between laser process parameters and joint forming quality indexes were established through RSM. Analysis of variance (ANOVA) was performed to evaluate the statistical significance of RSM models and the influence of process parameters on objectives. GA was adopted to obtain the optimal combination of laser process parameters considering multiple objectives.

2 FEA modeling of laser shock hole-clinching process

FEA model is established to perform the calculation scheme arranged by CCD, and then the combinations of process parameters and the corresponding FEA results are used to build RSM models. Some key issues need to be considered in FEA modeling, including the shock wave pressure loading, material property description, element type selection, and meshing plan.

2.1 Shock wave pressure loading

The peak value of laser-induced shock wave pressure P_{max} in the confining surrounding can be estimated by [25]

$$P_{max} = 10^{-9}\sqrt{\left(\frac{a}{2a+3}\right) \cdot Z \cdot I} \tag{1}$$

where a is the coefficient of energy conversion, and it is usually regarded as 0.1; Z is the shock impedance in relation to the interaction between the metal foil Z_1 and the confining overlay Z_2, expressed as $2/Z=1/Z_1+1/Z_2$; I is the laser power density depending on the pulsed laser energy E, the laser spot diameter D, and the pulse duration τ, expressed as $I = 4E/\pi D^2\tau$.

The temporal evolution of laser-induced shock wave pressure in FEA is shown in Fig. 3a. A triangular shape is adopted according to the changing history of laser pulse. The pressure is firstly increased to P_{max} at τ, and then it linearly decreases to zero within the next 2τ time. Figure 3b presents the spatial distribution of the pressure in FEA, which is generally considered a Gaussian pattern similar to that of laser beam. The pressure at the moment t and the position r can be expressed as $P_{(r,t)}=P_{(t)}\exp\left(-r^2/2r_0^2\right)$, in which r_0 is the radius of laser spot [26]. The subroutine VDLOAD was employed to carry out the shock wave pressure loading in FEA.

2.2 Material property description

The average strain rate of metal sheet in laser shock forming is as high as 10^3/s, which mainly relates to the laser process parameters and the specimen dimensions [27]. In this high-strain-rate range, the classical Johnson–Cook constitutive model is usually adopted to describe the material mechanical property [28]. It is noted that the formation of the joint in laser shock hole-clinching completely results from the effect of laser-induced shock wave, and thus the temperature softening item in Johnson–Cook model can be omitted. Therefore, the constitutive model can be written as

$$\sigma = (A + B\varepsilon^n)(1 + C\ln\frac{\dot{\varepsilon}}{\dot{\varepsilon}_0}) \tag{2}$$

where σ is the yield strength of metal foil; ε is the plastic strain; $\dot{\varepsilon}$ is the strain rate; $\dot{\varepsilon}_0$ is the reference strain rate; and A, B, and C are variables related to the specific joining partners. Since it has been proved that the formation of the joint entirely depends on the plastic deformation of the joining partner I, the joining partner II is regarded as a rigid body in FEA due to its relatively high strength. In the present work, T2 pure copper foil serves as the joining partner I, and the parameters of the Johnson–Cook model are as follows: $A=90$ MPa, $B=292$ MPa, $C=0.025$, and $n=0.31$ [29].

2.3 Finite element modeling

ABAQUS software was employed to implement FEA of laser shock hole-clinching due to its ability to solve highly nonlinear problems, especially under high strain rates. An axisymmetric simplification was adopted, because the geometrical configurations of both laser spot and pre-pierced hole on the joining partner II were circular. Element CAX4R, a 4-node reduced-integration axisymmetric solid element, was applied to mesh the joining partner I. In addition, the meshes of the region directly affected by shock wave pressure on the joining partner I were refined both in z and r directions in order to better capture the clinching behavior of metal foils. Figure 4 shows the schematic of established FEA model of laser shock hole-clinching.

3 Experimental procedure

The purpose of experiments is to verify both the established FEA model and the optimal combination of laser process parameters through GA. A Nd:YAG laser system (Nimma-series, Beamtech Optronics Co., Ltd.) was employed to implement the laser shock hole-clinching

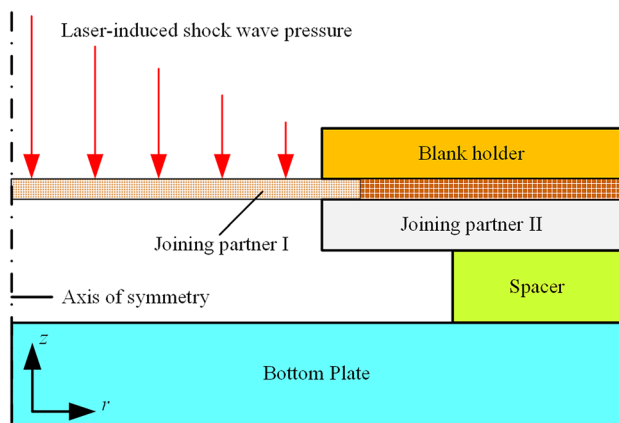**Fig. 3** Characteristics of shock wave pressure in FEA. **a** Temporal evolution; **b** spatial distribution

Fig. 4 FEA model of laser shock hole-clinching

4 Design of experiments for fitting response surface
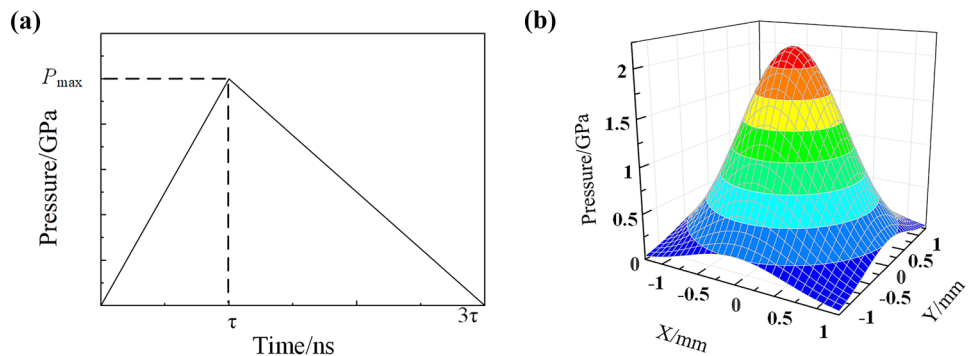
experiments. The output laser energy was measured using a digital energy meter (FieldMaxII-TOP, Coherent). Optical quartz glass was chosen to act as the confining layer due to its good transparency and high stiffness. Ink was used as the absorbent coating because of its high energy-absorbing ability and easy removal after clinching process. Before experiments, the ink was carefully pre-coated on the glass surface facing the metal foil until it completely solidified. Table 1 presents the detailed process parameters in experiments.

In experiments, T2 pure copper with the thickness of 30 μm and 304 stainless steel with the thickness of 100 μm were used to act as the joining partner I and II, respectively. The hole on steel foil was manufactured by a fiber laser cutting machine (SF3015, Senfeng Laser Technology Co., Ltd.). The as-received pure copper foil was annealed in a vacuum furnace at the temperature of 450 °C for 1 h to eliminate the rolling direction effect.

Table 1 Detailed process parameters in experiments

Parameter	Unit	Value
Laser wavelength	nm	1064
Pulse duration	ns	7.3
Pulse frequency	Hz	1
Thickness of quartz glass	mm	3
Thickness of ink	μm	~80
Thickness of T2 pure copper foil	μm	30
Initial grain size of T2 pure copper foil	μm	12
Thickness of 304 stainless steel foil	μm	100
Pre-pierced hole diameter	mm	2.0
Spacer height	μm	150
Pulsed laser energy (E)	mJ	145–165
Number of laser pulses (N)	/	18–26
Laser spot diameter (D)	mm	1.9–2.1

The goal of RSM is to build an explicit function which links the joint forming quality indexes to laser process parameters, and then the proposed model can conveniently predict the clinching results in various laser shock conditions instead of experiments and numerical simulations. Moreover, the established RSM model is used in the subsequent GA optimization to obtain the solutions of populations during iterations.

RSM is a compilation of mathematical and statistical techniques that are used for the modeling and analysis of the problem in which a response is influenced by many quantifiable variables. With the established RSM models, it can predict the relationship between the controlling variables and the concerned responses in a specific range. In addition, it can be used for finding the critical controlling variables which significantly affect the response. A representative RSM contains the design of experiments, the establishment of an empirical model, and the statistical analysis of the built model [30].

For clinching and laser shock processes, the second-order RSM model is usually adopted to identify the relationship between the variable x and the response $y(x)$

$$y(x) = \beta_0 + \sum_{i=1}^{n} \beta_i x_i + \sum_{i=1}^{n} \beta_{ii} x_i^2 + \sum_{i<j}^{n} \beta_{ij} x_i x_j \qquad (3)$$

where β_0, β_i, β_{ii}, and β_{ij} are coefficients of the fitted response surface.

The design of experiments is essential for RSM modeling, and the choice of the controlling variables and responses needs to be carefully treated. In laser shock hole-clinching process, both the pulse duration and laser wavelength directly relate to the applied laser system, and thus they are usually kept constant in the process. Pulse frequency is generally in the range of 1–10 Hz for a Nd:YAG laser, but the high frequency may make the laser system overheating when lots of laser pulses are applied. The pulsed laser energy, number of laser pulses, and laser spot diameter are easy to adjust, and thus they are usually selected as changeable variables in practice aiming at different clinching requirement.

In our previous research, it is observed that the too low laser energy is unable to generate required plastic deformation of the joining partner I, but the facture will appear prior to the formation of joint with the too high laser energy. The determination of the necessary laser energy has a strong correlation with the mechanical properties of the joining partners, and meanwhile the clinching efficiency should also be considered. Therefore, we performed the FEA of laser shock hole-clinching at $E = 130$ and 180 mJ, and the results after 25 pulses are shown in

Fig. 5. It is found that the interlock value (t_S) is as low as 6.60 µm at $E = 130$ mJ after 25 pulses, implying that further laser pulses are needed to enlarge the value, as seen in Fig. 5a. The t_S dramatically increases to 44.18 µm as the laser energy is enhanced to 180 mJ, whereas it is noted that the maximum thinning rate (η_{max}) is as high as 68.33% (refer to Fig. 5b). It is obvious that the excessively high thinning may lead to the degradation of joint strength and even the premature occurrence of fracture in service. According to the above results, the range of 145–165 mJ is available for pulsed laser energy in the case of pure copper foil of 30 µm in thickness.

The reasonable number of laser pulses should maintain the balance between the joint forming quality and the clinching efficiency. Figure 6 shows a typical relationship between the number of laser pulses and interlock value at $E = 155$ mJ and $D = 2.0$ mm. It can be seen that there is no clear evidence of interlock formation while $N < 15$. When 17 pulses have been applied, the t_S of about 5 µm is achieved, and it increases almost linearly under the effect of further pulses. It is noted that while 27 pulses have been exerted, the maximum thinning rate reaches 56.77%, which may weaken the load capacity of the joint if it continues to increase. For the given process parameters in Table 1, the range of 18–26 for N was adopted for RSM modeling.

The determination of laser spot diameter needs to deal with two conflicting issues. A small spot is helpful to enhance the amplitude of shock wave pressure, but it reduces the directly affected area of laser beam on metal foils. On the other side, an oversize spot may lead to the punching if the pulsed laser energy is high enough [31]. In addition, the
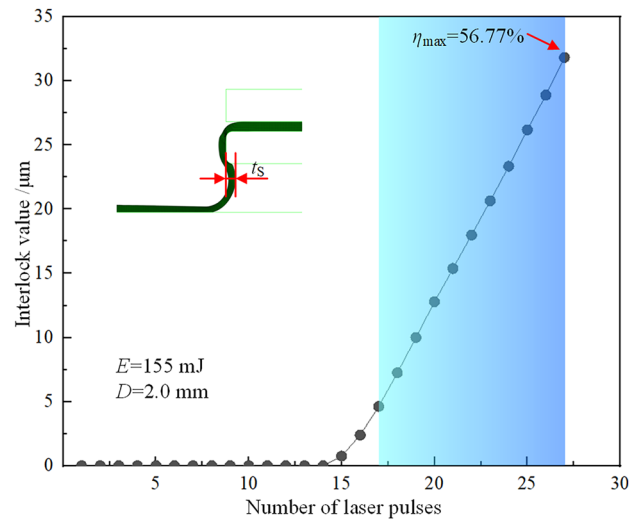

Fig. 6 Relationship between the number of laser pulses and interlock value

relationship of spot diameter to pre-pierced hole diameter also needs to be considered. In the case of the pre-pierced hole diameter of 2.0 mm, the laser spot diameter of 1.9, 2.0, and 2.1 mm was chosen for study, which represents the ratio of spot diameter to pre-pierced hole diameter of < 1, $= 1$, and > 1.

Besides the three controlling variables, the response of RSM model should also be identified. Obviously, t_S needs to be considered, because it directly relates to the fact whether the connection is successful or not. As seen in Fig. 5, although the laser energy is increased from 130 to 180 mJ, it is noted that the change of neck thickness
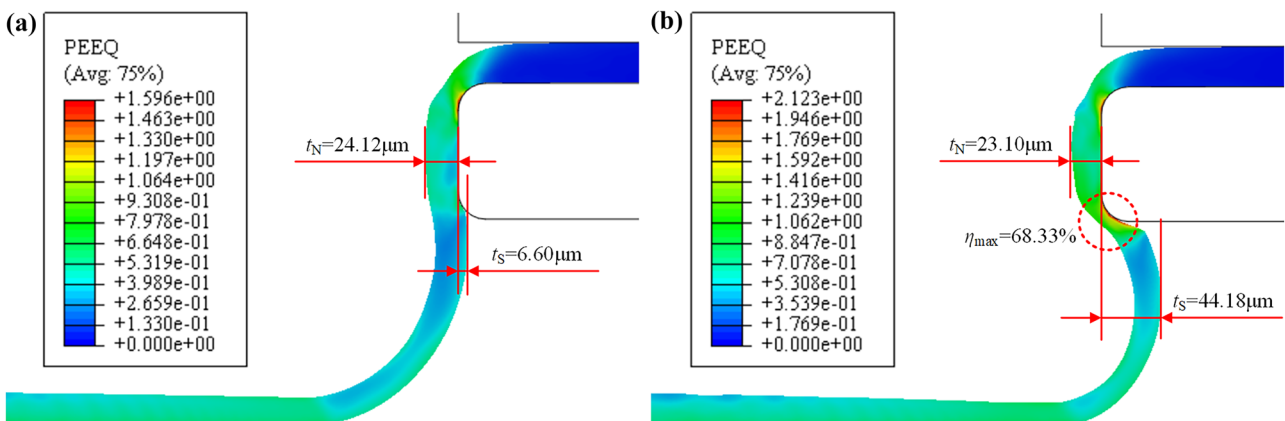

Fig. 5 FEA result in the clinched region after 25 pulses under various pulsed laser energies. **a** $E = 130$ mJ; **b** $E = 180$ mJ
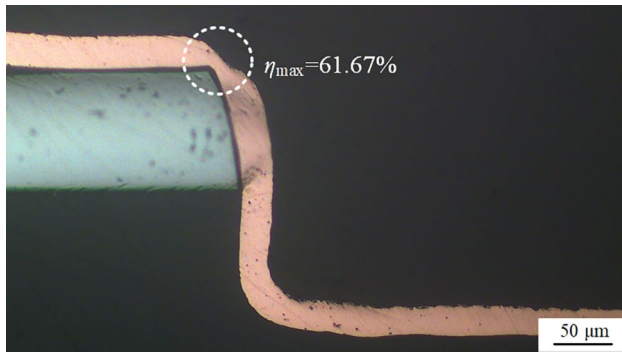
Fig. 7 Local thinning in the clinched joint

(t_N) is quite small. In fact, among the process parameters in Table 1, t_N varies little, and it is always more than 20 µm according to FEA results, so we do not take it as a response.

In addition, it is noted that some positions in the FEA result of Fig. 5b and the experimental observation of Fig. 7 exhibit excessive thinning, suggesting that the thinning rate is important and needs to be assessed for joint forming quality. The thinning rate η is expressed by

$$\eta = \frac{h_0 - h}{h_0} \times 100\% \tag{4}$$

where h_0 and h are the thickness of the joining partner I before and after hole-clinching, respectively. It is obvious that the maximum thinning rate (η_{max}) is crucial to the joint forming quality, and thus it is chosen as another response of RSM models.

While both the controlling variables and the responses have been identified, an experimental design needs to be carried out. Central composite design (CCD) is one of the most acceptable design methods for RSM modeling, and it is used to arrange the simulation scheme using the established FEA model [22, 32]. For each variable, three levels are used, and their values are listed in Table 2. The combinations of variables through CCD are summarized in Table 3, which will be numerically simulated in sequence.

Table 2 Design variables and their levels

Variable	Illustration	Unit	Levels		
			1	2	3
E	Pulsed laser energy	mJ	145	155	165
N	Number of laser pulses	/	18	22	26
D	Laser spot diameter	mm	1.9	2.0	2.1

Table 3 Central composite design matrix and FEA results

Exp. no.	E (mJ)	N	D (mm)	t_S (µm)	η_{max} (%)
1	165	26	1.9	25.52	46.35
2	165	18	2.1	8.22	55.14
3	155	22	2.0	17.98	50.08
4	155	22	2.1	16.27	59.63
5	155	26	2.0	28.90	52.00
6	145	18	2.1	1.43	51.01
7	155	18	2.0	7.26	48.38
8	145	26	1.9	18.60	43.75
9	145	18	1.9	0.94	38.14
10	145	22	2.0	11.41	48.22
11	165	22	2.0	21.08	50.87
12	145	26	2.1	20.95	58.43
13	155	22	1.9	13.31	43.06
14	165	26	2.1	33.88	62.97
15	165	18	1.9	3.54	39.22

5 Results and discussion

5.1 Validation of FEA model

Figure 8 presents the comparison of FEA and experimental measurements in terms of t_S and t_N. The laser process parameters are as follows: $E = 155$ mJ, $D = 2.0$ mm, $N = 25$. It is distinctly seen that an interlock structure has been produced after a total number of 25 pulses for both FEA and experiments. The t_S is 24.35 µm in the experiment, while it is 26.24 µm in FEA. The t_N is 26.49 µm from experiments, compared with 23.80 µm from FEA. As a result, it is concluded that the FEA results have a good consistency with those of experiments, demonstrating that the established FEA model is reliable, and it can be employed to carry out the numerical simulation scheme arranged by CCD.
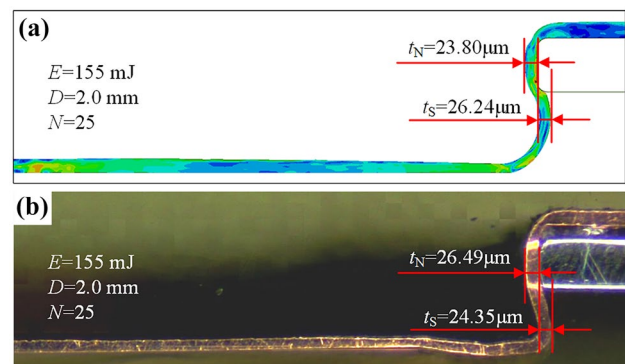

Fig. 8 Comparison of FEA (**a**) and experimental measurements (**b**)

The deviation between FEA and actual results is mainly attributed to the difference in the mechanical properties of metal foils and the manufacturing tolerance of pre-pierced hole on the stainless steel foil.

5.2 Establishment of response surface model

Table 3 shows the combinations of laser process parameters and their FEA results according to the CCD matrix. Design Expert software was used to perform the experimental design, and each experimental plan was implemented by using the validated FEA model. Both t_S and η_{max} were measured from FEA results, and their values were also summarized in Table 3. In addition, it can be seen that t_S varies dramatically in the range of 0.94 to 33.88 μm, while η_{max} changes from 38.14 to 62.97%, implying that the optimization of controlling variables is quite necessary in the given design space. Moreover, it is noticeable that in some cases, η_{max} is larger than 60%, suggesting that these combinations are unreasonable and should be taken out in the next optimization.

Based on the data from Table 3, the coefficients of Eq. (3) can be calculated by using MATLAB software. Therefore, the mathematical models of responses in terms of t_S and η_{max} are

5.3 Response surface analysis of laser process parameters

The assessment of the established RSM models is necessary in order to test the prediction ability of models in the design space. ANOVA is a well-known powerful way to perform statistical analysis to evaluate the significance of established RSM models and the influence of controlling variables on responses. Moreover, the determination coefficient R^2, the adjusted coefficient R^2_{adj}, the predicted coefficient R^2_{pred}, and signal-to-noise ratio are also widely used to evaluate the fitting precision of the models.

5.3.1 Interlock value

Table 4 presents the ANOVA and fitting precision analysis of the RSM model of interlock value. The F value of 233.66 for the model indicates that the model is statistically significant. The F values of E, N, and D are 229.65, 1719.13, and 53.84, respectively, indicating that the influence order of these parameters on interlock value

$$t_S = -953.7913 + 1.1483 \times E - 7.3403 \times N + 884.9053 \times D + 0.0327 \times E \times N \tag{5}$$
$$+ 1.2750 \times E \times D + 1.7313 \times N \times D - 0.0130 \times E^2 + 0.0335 \times N^2 - 275.4444 \times D^2$$

$$\eta_{max} = 25.8712 + 2.5553 \times E - 0.1290 \times N - 268.8331 \times D + 0.0060 \times E \times N \tag{6}$$
$$+ 0.6238 \times E \times D + 0.7844 \times N \times D - 0.0122 \times E^2 - 0.0360 \times N^2 + 57.8889 \times D^2$$

Table 4 ANOVA and fitting precision analysis for interlock value

ANOVA for interlock value							
Source	Sum of squares	df	Mean square	F value	P value		C %
Model	1386.41	9	154.05	233.66	<0.0001	Significant	
E	151.40	1	151.40	229.65	<0.0001		10.93
N	1133.37	1	1133.37	1719.13	<0.0001		82.16
D	35.49	1	35.49	53.84	0.0007		2.53
$E \times N$	13.68	1	13.68	20.74	0.0061		0.94
$E \times D$	13.01	1	13.01	19.73	0.0068		0.90
$N \times D$	3.84	1	3.84	5.82	0.0607		0.23
E^2	4.34	1	4.34	6.59	0.0503		0.27
N^2	0.74	1	0.74	1.12	0.3386		0.01
D^2	19.51	1	19.51	29.59	0.0028		1.37
Residual	3.30	5	0.66				
Cor total	1389.71	14					
Fitting precision analysis for interlock value							
R^2			0.9976				
R^2_{adj}			0.9934				
R^2_{pred}			0.9750				
Signal-to-noise ratio			49.79				

from strong to weak is N, E, and D. For each model term, the P value < 0.05 means that this model term is statistically significant. Thus, E, N, D, $E \times N$, $E \times D$, and D^2 are significant model terms associated with the interlock value. The R^2 of $0.9976 > 0.9$ suggests that the established model completely satisfies the accuracy requirement. The difference between R^2_{pred} (0.9750) and R^2_{adj} (0.9934) is less than 0.2, which further demonstrates the high fitting precision of the model [33]. For RSM models, it is desirable that the signal-to-noise ratio is greater than 4, and it is found that this ratio of interlock value model is as high as 49.79. This value indicates an adequate signal, suggesting that this model can be used to navigate the given design space of variables. The comparison of predicted and actual interlock values also proves that the mathematical model is able to predict the actual data, as seen in Fig. 9.

Figure 10 presents 3D surface graphs and contour maps for t_S in terms of different pairs of variables, which identify the interaction of two variables, while another one remains unchanged.

As shown in Fig. 10a, b, it can be seen that both a higher pulsed laser energy and more laser pulses are beneficial to obtaining a larger interlock value. Obviously, it is reasonable that more deformation e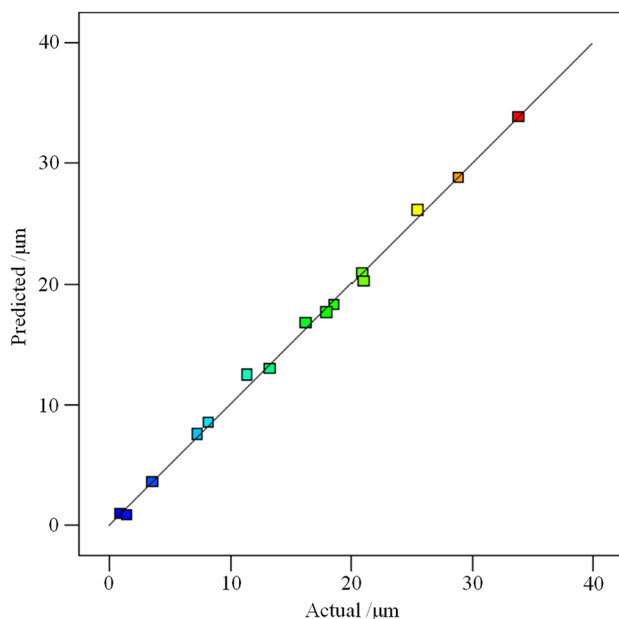nergies can be available for metal foils in these cases. In addition, it is noted that in comparison to E, the variation of N results in a greater change of interlock value (refer to Fig. 10a). For contour maps, the more circular the contour is, the less significant the interaction of the two variables is. Thus, both the relatively gentle distribution and the nearly circular shape of contours in Fig. 10b indicate that there is no significant interaction effect between E and N.

Figure 10c apparently presents that the influence of laser spot diameter on interlock value is different from those of the other two variables. When a low-level laser energy is applied, the highest point of interlock value almost locates at the middle of D. The highest point moves to $D = 2.05$ mm, while E is in high level. Therefore, this phenomenon means that neither too large nor too small spot diameter is preferable to a considerable interlock value, but the most appropriate D value is easily captured from the response plots. An elliptical shape in Fig. 10d illustrates that the interaction effect of E and D exists.

Figure 10e depicts that the interlock value is more sensitive to change in N than to change in D. From the examination of the contour map in Fig. 10f, it is concluded that there is no significant interaction effect between N and D.

5.3.2 The maximum thinning rate

The ANOVA and fitting precision analysis of the maximum thinning rate model are shown in Table 5. The F value of 64.84 suggests that the established model is statistically significant. The F values of E, N, and D are 18.22, 80.90, and 475.84, respectively, indicating that the influence order of three parameters on the maximum thinning rate from strong to weak is D, N, and E.

Moreover, from Table 5, it is found that E, N, and D are significant model terms associated with the maximum thinning rate due to the P value < 0.05. The $R^2 > 0.9$ suggests that the established model completely satisfies the accuracy requirement. The difference between R^2_{pred} (0.9243) and R^2_{adj} (0.9762) is less than 0.2, which further demonstrates the high fitting precision of the model. In addition, the signal-to-noise ratio is 27.17, suggesting that this model can be used to navigate the given design space of variables. The comparison of predicted and actual maximum thinning rate also proves that the RSM model can be used to predict the practical result, as seen in Fig. 11.
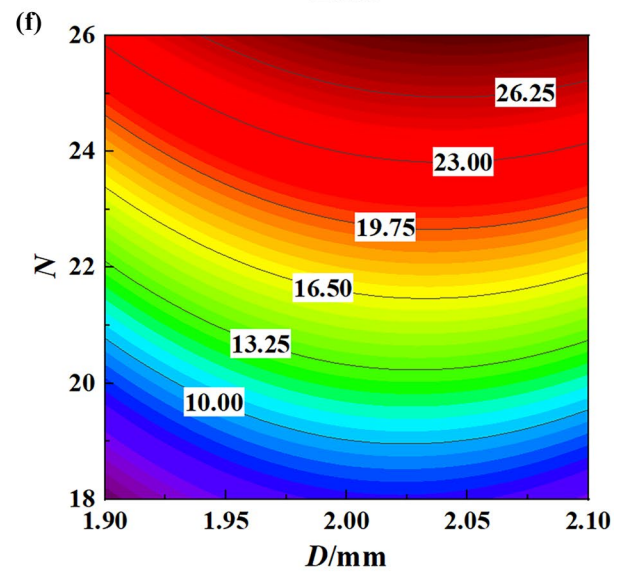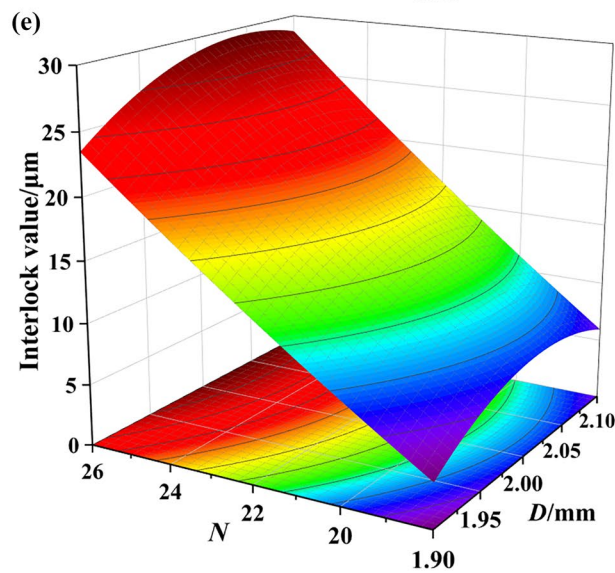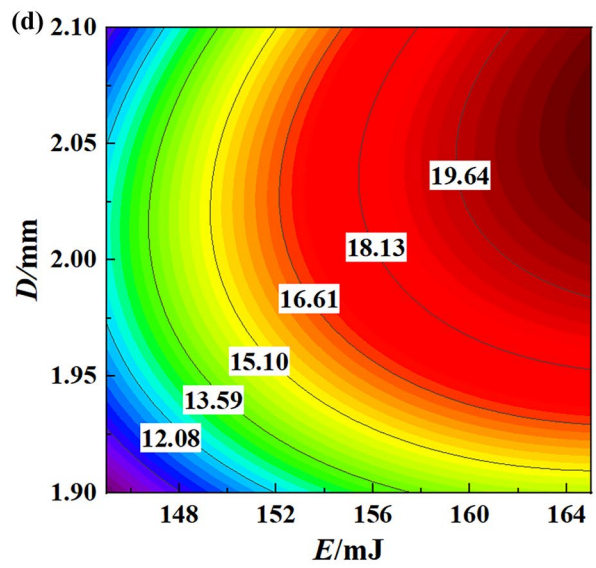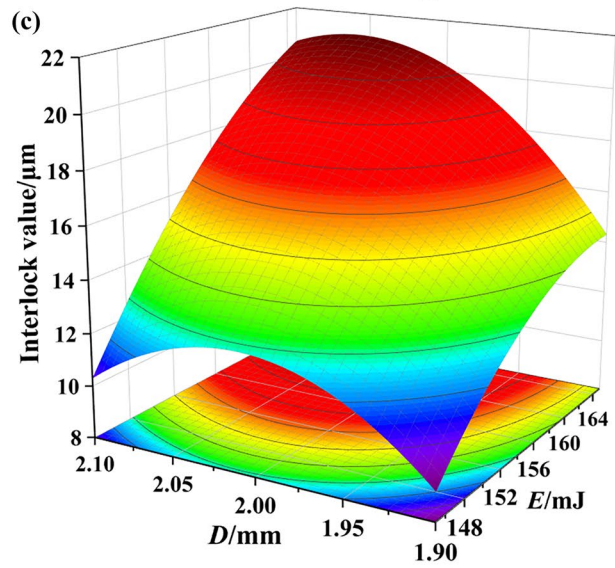

Fig. 9 Comparison of predicted and actual interlock value

(a)

(b)

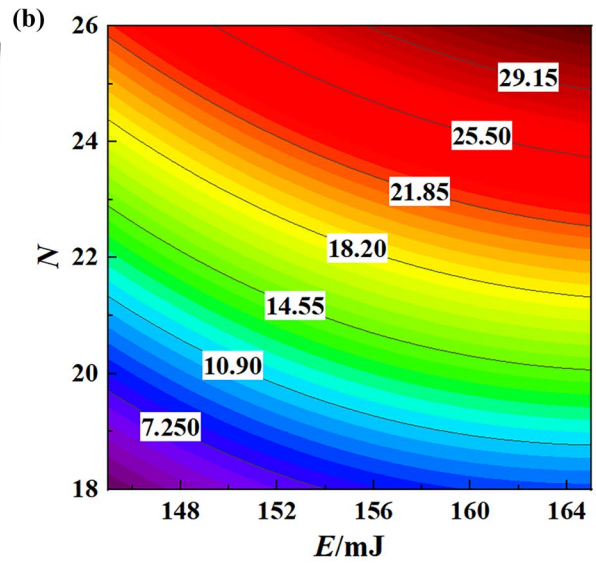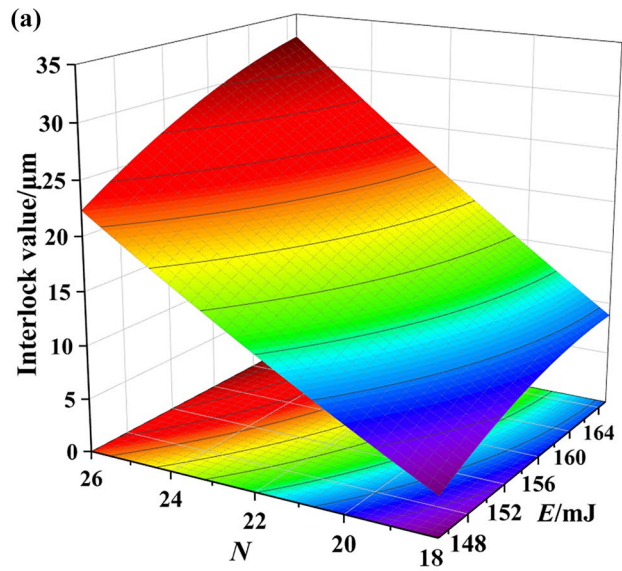

(c)

(d)

(e)

(f)

◄**Fig. 10** 3D surface graphs and contour maps for interlock value. **a**, **b** Interaction effect of E and N at $D=2.0$ mm; **c**, **d** interaction effect of E and D at $N=22$; **e**, **f** interaction effect of N and D at $E=155$ mJ

Figure 12 shows 3D surface graphs and contour maps for η_{max} in terms of different pairs of variables. As shown in Fig. 12a, b, the more both pulsed laser energies and laser pulses are, the larger the maximum thinning rate is. Due to the fact that the formation of joint is attributed to the bulging forming of metal foil under laser shock, the thickness of metal foil decreases gradually with the action of biaxial tensile stresses. While more laser energies and laser pulses are applied, the deformation amount of metal foil becomes larger, leading to a bigger reduction in thickness. Furthermore, the variation of N brings about a greater increase in the maximum thinning rate compared with E, as seen in Fig. 12a. A slightly elliptical shape in Fig. 12b indicates that there is a weak interaction effect between E and N.

Figure 12c reflects that the maximum thinning rate is more sensitive to change in D than to change in E. Due to the expression of $I = 4E/\pi D^2\tau$, the influence of D squared on I is apparently stronger than that of E, which further has a greater impact on P_{max} according to Eq. (1). Therefore, while D enlarges from 1.9 to 2.1 mm, η_{max} exhibits rapid growth from 43 to about 60% when E is in high level. The relatively gentle distribution of contours in Fig. 12d illustrates that there is no significant interaction effect between E and D.

Figure 12e presents that the change in D plays a more important role on the maximum thinning rate than that of N. In addition, the relatively gentle distribution of contours in Fig. 12f exhibits that there is no significant interaction effect between N and D.

5.4 Genetic optimization of laser process parameters

The interlock value directly relates to the fact that whether the laser shock hole-clinching process is successful or not, the maximum thinning rate is involved with the load capacity of the joint. A large η_{max} is expected, because it generally means that the considerable plastic deformation has occurred. However, under certain circumstances although the η_{max} is quite large, the interlock structure still fails to be obtained, as seen in Fig. 7. It confirms that the simultaneous optimization of t_S and η_{max} is necessary. Therefore, the optimization aims at maximizing both the t_S and η_{max} in the given variables space under the constraints. According to our experiments, a joint with a small t_S is easy to be pulled out, and thus at least 10 μm of t_S is set in the optimization. The η_{max} of joint obviously needs to be controlled lower than 60% (refer to Figs. 5 and 7). On the other side,

Table 5 ANOVA and fitting precision analysis for the maximum thinning rate

ANOVA for the maximum thinning rate

| Source	Sum of squares	df	Mean square	F value	P value		C %
Model	720.76	9	80.08	64.84	0.0001	Significant	
E	22.50	1	22.50	18.22	0.0080		2.93
N	99.92	1	99.92	80.90	0.0003		13.59
D	587.68	1	587.68	475.84	<0.0001		80.76
$E \times N$	0.47	1	0.47	0.38	0.5661		0.11
$E \times D$	3.11	1	3.11	2.52	0.1733		0.26
$N \times D$	0.79	1	0.79	0.64	0.4608		0.06
E^2	3.83	1	3.83	3.10	0.1384		0.36
N^2	0.85	1	0.85	0.69	0.4437		0.05
D^2	0.86	1	0.86	0.70	0.4416		0.05
Residual	6.18	5	1.24				
Cor Total	726.93	14					
Fitting precision analysis for the maximum thinning rate							
R^2			0.9915				
R^2_{adj}			0.9762				
R^2_{pred}			0.9243				
Signal-to-noise ratio			27.17				
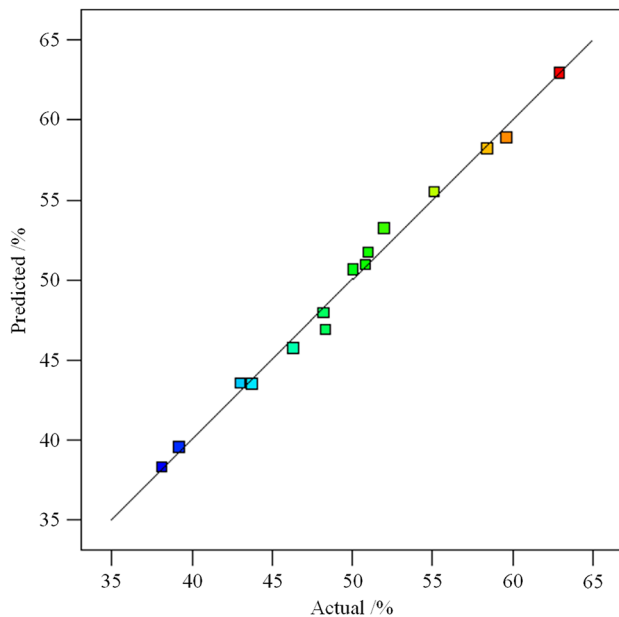
Fig. 11 Comparison of predicted and actual maximum thinning rate

according to Table 3, the η_{max} in the given variables space is larger than 38%, so at least 40% of η_{max} is required in order to accelerate the optimization. Table 6 presents the optimization criteria with a collection of variables, constraints, and objectives.

MATLAB software was employed to implement the GA multi-objective optimization. The population size was set as 200. For an individual of the population, it contains a specific combination of E, N, and D. The established RSM models were called to calculate t_S and η_{max} for each population. Selection, crossover and mutation are three main operators in GA, which was conducted in order within each iteration. In the present work, the roulette wheel selection was adopted, and one cut-point crossover was carried out with the probability of 0.7. Bit-flip mutation was performed with the probability of 0.03. The whole optimization lasted for 50 iterations, and the optimization histories of two objectives are shown in Fig. 13.

For a multi-objective optimization problem, it means that two or more conflictive objectives need to be optimized at the same time. A difficulty lies in the fact that getting better in one objective often leads to getting worse in another one. Therefore, the target of the multi-objective optimization is aimed to obtain a set of solutions that they are not worse for all objective, which is the well-known Pareto noninferior solutions

Fig. 12 3D surface graphs and contour maps for the maximum thinning rate. **a**, **b** Interaction effect of E and N at $D = 2.0$ mm; **c**, **d** interaction effect of E and D at $N = 22$; **e**, **f** interaction effect of N and D at $E = 155$ mJ

[34]. Table 7 presents the 32 groups of Pareto noninferior solutions after 50 iterations.

In order to comprehensively evaluate the Pareto noninferior solutions, the satisfaction function F_{sat} is employed to find the best optimal combination of variables [22, 35]

$$F_{sat} = \frac{f_1 - f_{1min}}{f_{1max} - f_{1min}} + \frac{f_2 - f_{2min}}{f_{2max} - f_{2min}} \tag{7}$$

where f_1 and f_2 represent t_S and η_{max} of each solution, respectively. $f_{1max}, f_{2max}, f_{1min}$, and f_{2min} are the maximum and minimum values of f_1 and f_2 among the Pareto noninferior solutions. The calculated satisfaction function values of Pareto solutions set are also summarized in Table 7. A bigger F_{sat} is expected in order to maximize both t_S and η_{max}. Therefore, the best optimal solution can be obtained, as listed in Table 8. The corresponding t_S and η_{max} of the best solution by RSM-GA optimization are 31.14 µm and 59.31%, respectively.

5.5 Confirmation test

A confirmation test was performed in order to verify the optimization result through both FEA and experimental approaches. Due to the fact that the energy resolution of the used laser system is 1 mJ and the spot diameter of 2.07 mm is inconveniently adjusted in practice, the best optimal parameters are rounded, as seen in Table 8. Based on the rounding values, both FEA and experiment were conducted, and the results are presented in Fig. 14. It can be apparently seen that a joint with a good configuration has been achieved with the aid of optimization technique.

Table 9 summarizes the t_S and η_{max} values from different sources. As shown in Table 9, it is noted that the difference between the results of RSM-GA optimization and experiment is 13.65% and 3.63%, suggesting that the established multi-objective optimization model is reliable for laser shock hole-clinching process. Moreover, the small deviation between the results of RSM-GA optimization and FEA further confirms the effectiveness of the established RSM models, which provides a feasible way to save time and effort in the development of laser shock hole-clinching process.
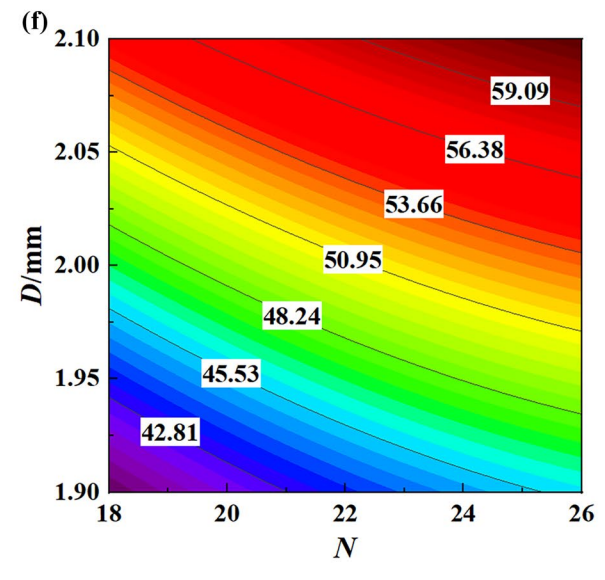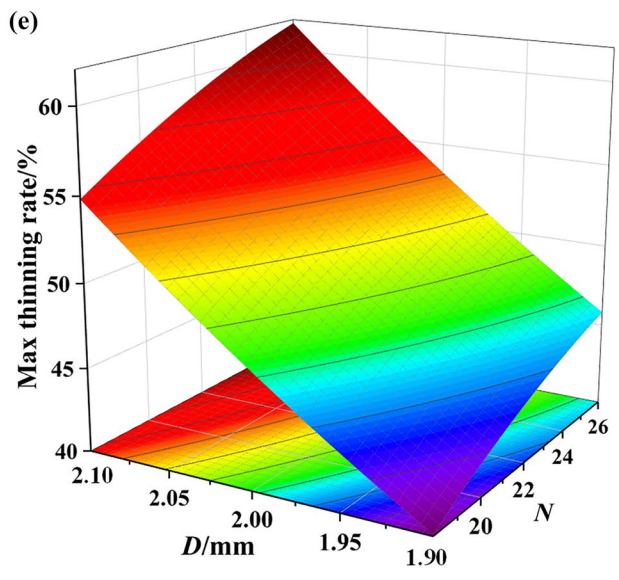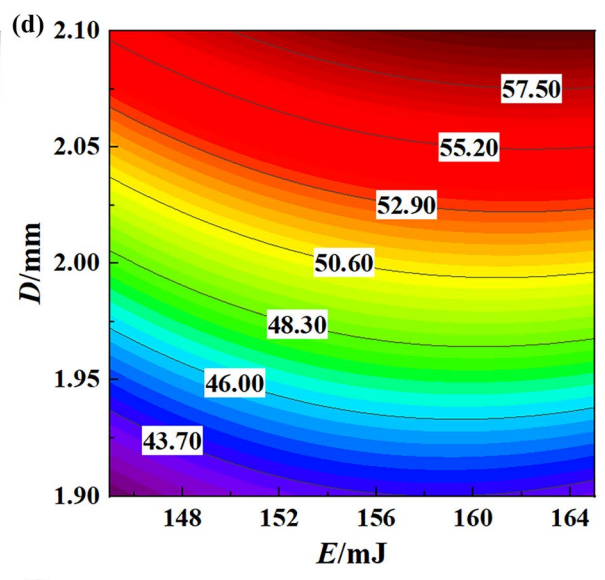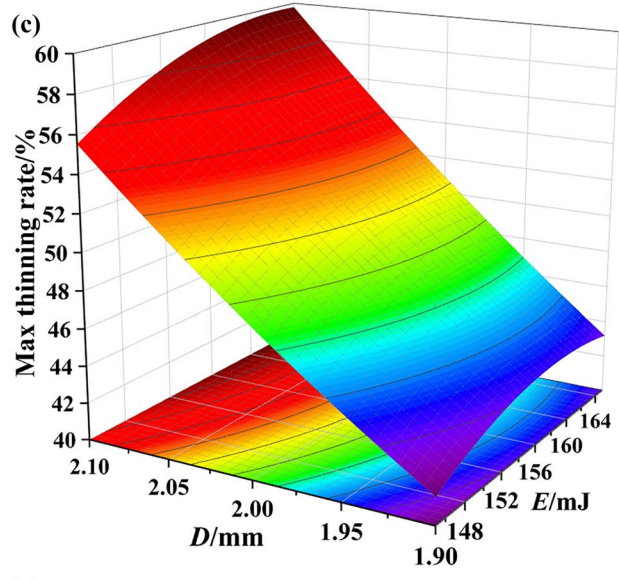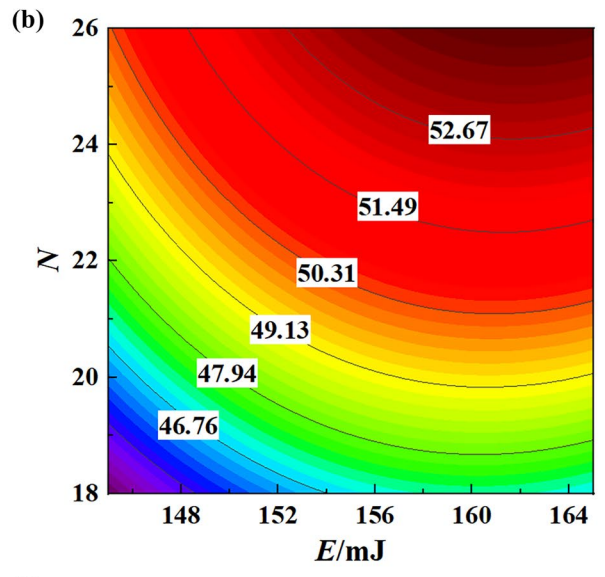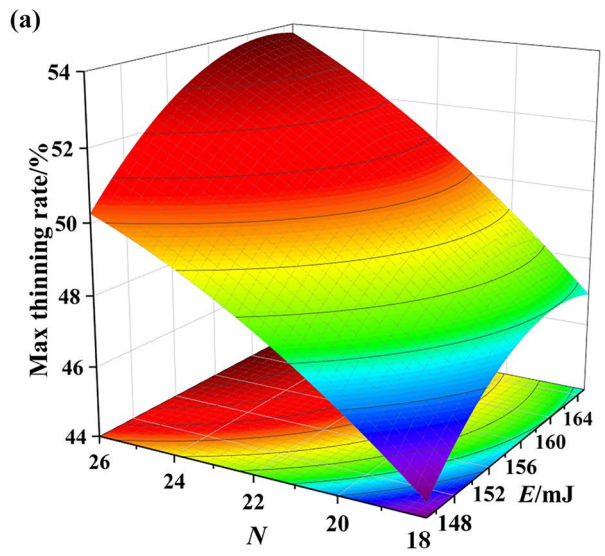
Table 6 Optimization criteria

Categories	Parameters	Bound		Directions
		Lower	Upper	
Variables	E (mJ)	145	165	
	N	18	26	
	D (mm)	1.9	2.1	
Constraints	t_S (μm)	10		
	η_{max} (%)	40	60	
Objectives	t_S			Maximize
	η_{max}			Maximize

Table 8 The best optimal parameters according to satisfaction function

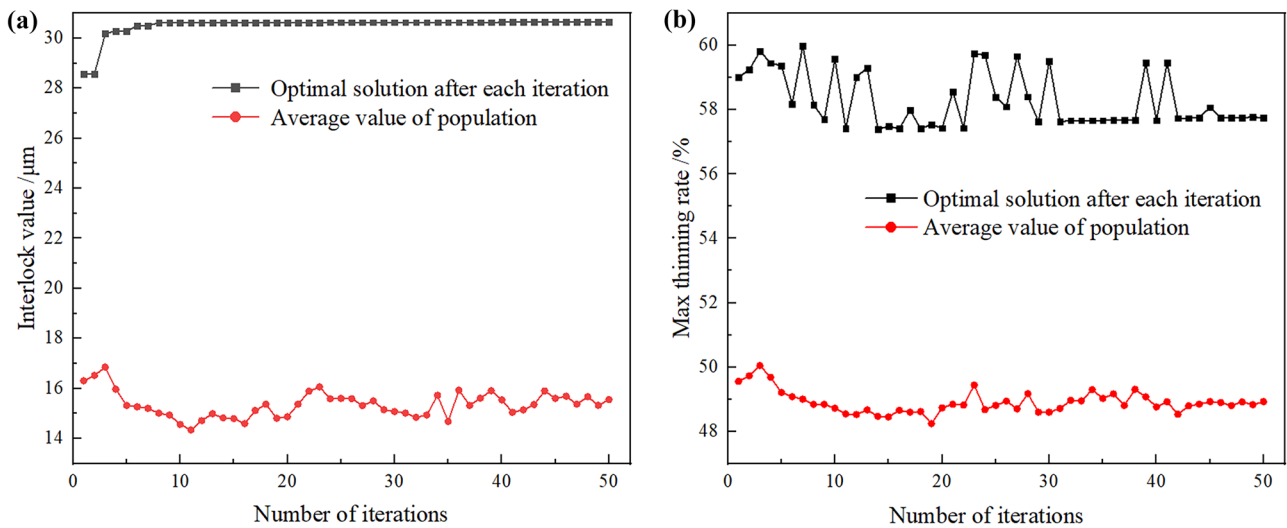| Parameters	E (mJ)	N	D (mm)
The best optimal solution	163.75	25	2.07
Rounding values	164	25	2.1

Fig. 13 Optimization histories of objectives. **a** Interlock value; **b** the maximum thinning rate

Table 7 Pareto noninferior solutions and corresponding satisfaction function values

No.	E (mJ)	N	D(mm)	F_{sat}	No.	E (mJ)	N	D(mm)	F_{sat}
1	160	25	2.04	1.78	17	145.01	18	1.96	0.01
2	165	25	2.04	1.84	18	145.01	18.44	1.96	0.06
3	163.75	25	2.03	1.82	19	145.01	18	1.96	0.01
4	165	24.55	2.04	1.77	20	145.01	18	1.96	0.01
5	160	25	2.04	1.78	21	145.01	18	1.96	0
6	165	25	2.04	1.84	22	145.03	18	1.96	0.01
7	165	25	2.04	1.84	23	145.01	18	1.96	0.01
8	165	25	2.04	1.84	24	145.01	18	1.96	0.01
9	163.75	24.98	2.04	1.83	25	145.01	18	1.96	0.01
10	163.75	25	2.04	1.83	26	145.01	18	1.96	0.01
11	163.75	24.99	2.01	1.66	27	145.01	18	1.96	0.01
12	160	25	2.07	1.93	28	145.01	18	1.96	0.01
13	162.5	25	2.04	1.82	29	145	18.22	1.96	0.03
14	163.75	25	2.07	1.99	30	164.99	18	1.94	0.15
15	165	25	2.04	1.84	31	145.01	18	1.96	0.01
16	160	25	2.07	1.93	32	145.01	18	1.96	0.01

Fig. 14 Comparison of experimental and numerical results using the best optimal parameters
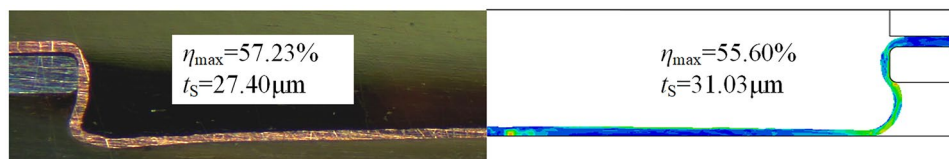

Table 9 Comparison of two objectives from different sources

Sources	t_S (μm)	Deviation (%)	η_{max} (%)	Deviation (%)
Experiment	27.40	\	57.23	\
FEA	31.03	13.25	55.60	−2.85
RSM-GA optimization	31.14	13.65	59.31	3.63

6 Conclusions

In this paper, the mathematical models between laser process parameters and joint quality indexes were established through RSM. ANOVA was performed to assess the statistical significance of RSM models and the influence of process parameters on objectives. Multi-objective optimization was carried out to obtain the optimal combination of laser process parameters by using GA. The following conclusions are drawn from this research:

1. The RSM-GA-integrated approach has been proposed which realizes the modeling and optimization of laser process parameters for laser shock hole-clinching. The prediction accuracy of RSM models and the optimization result by means of GA are confirmed through experiments.
2. The pulsed laser energy, number of laser pulses, and laser spot diameter are statistically significant, and both the interlock value and the maximum thinning rate are sensitive to these parameters based on ANOVA. Therefore, it is necessary for laser process parameters to be modeled and optimized, while metal foils with different classification and thickness are joined by laser shock hole-clinching process.
3. The influence order of laser process parameters on interlock value from strong to weak is N, E, and D, while this order changes to D, N, and E for the maximum thinning rate.
4. In the joining of T2 pure copper and 304 stainless steel foils with the thickness of 30 and 100 μm, the optimal parameters combination is $E = 164$ mJ, $N = 25$, and $D = 2.1$ mm.

Additionally, the present research focuses on the modeling and optimization of laser process parameters in laser shock hole-clinching. Although the established RSM models exhibit relatively high prediction accuracy, other surrogate model methods, such as ANN, deserve further attempt to improve the predictive ability of the complicated nonlinear problem. Moreover, besides laser process parameters, the height and diameter of spacer, the pre-pierced hole diameter, and the thickness of joining partners are worth taken into consideration as design variables. In addition, the relationship between process parameters and joint strength needs to be carefully investigated as well as the modeling and optimization of joint strength.

Declarations

References

1. Righi G, Ruestes CJ, Stan CV, Ali SJ, Rudd RE, Kawasaki M, Park HS, Meyers MA (2021) Towards the ultimate strength of iron: spalling through laser shock. Acta Mater 215:117072. https://doi.org/10.1016/j.actamat.2021.117072
2. Groche P, Wohletz S, Brenneis M, Pabst C, Resch F (2014) Joining by forming—a review on joint mechanisms, applications and future trends. J Mater Process Technol 214:1972–1994. https://doi.org/10.1016/j.jmatprotec.2013.12.022
3. Wang XY, Ji Z, Liu R, Zheng C (2018) Making interlock by laser shock forming. Opt Laser Technol 107:331–336. https://doi.org/10.1016/j.optlastec.2018.06.011
4. Veenaas S, Wielage H, Vollertsen F (2014) Joining by laser shock forming: realization and acting pressures. Prod Eng Res Devel 8:283–290. https://doi.org/10.1007/s11740-013-0521-z
5. Wang X, Li XD, Li C, Shen ZB, Ma YJ, Liu HX (2018) Laser shock micro clinching of Al/Cu. J Mater Process Technol 258:200–210. https://doi.org/10.1016/j.jmatprotec.2018.04.005
6. Li XD, Wang X, Shen ZB, Ma YJ, Liu HX (2019) An experimental study on micro-shear clinching of metal foils by laser shock. Materials 12:1422. https://doi.org/10.3390/ma12091422

7. Wang J, Wang YQ, Wang S, Lu GX, Zheng C, Ji Z (2021) Experimental and numerical investigation on incremental laser shock clinching for joining three sheets of copper/aluminum/stainless steel. Opt Laser Technol 141:107141. https://doi.org/10.1016/j.optlastec.2021.107141

8. Veenaas S, Vollertsen F (2015) Forming behavior during joining by laser induced shock waves. Key Eng Mater 651–653:1451–1456. https://doi.org/10.4028/www.scientific.net/KEM.651-653.1451

9. Zheng C, Pan CD, Tian ZR, Zhao XH, Zhao GQ, Ji Z, Song LB (2020) Laser shock induced incremental forming of pure copper foil and its deformation behavior. Opt Laser Technol 121:105785. https://doi.org/10.1016/j.optlastec.2019.105785

10. Wang XY, Ji Z, Wang JF, You SX, Zheng C, Liu R (2018) An experimental and numerical study on laser shock clinching for joining copper foil and perforated stainless steel sheet. J Mater Process Technol 258:155–164. https://doi.org/10.1016/j.jmatprotec.2018.03.025

11. You SX, Wang XY, Ji Z, Zheng C, Zhang GF, Liu R (2019) Making line undercut structure by incremental laser shock forming. Int J Precis Eng Manuf 20:1289–1296. https://doi.org/10.1007/s12541-019-00141-w

12. Lambiase F, Di Ilio A (2013) Optimization of the clinching tools by means of integrated FE modeling and artificial intelligence techniques. Procedia CIRP 12:163–168. https://doi.org/10.1016/j.procir.2013.09.029

13. Shen XJ, Shukla P, Subramaniyan AK, Zammit A, Swanson P, Lawrence J, Fitzpatrick ME (2020) Residual stresses induced by laser shock peening in orthopaedic Ti-6Al-7Nb alloy. Opt Laser Technol 131:106446. https://doi.org/10.1016/j.optlastec.2020.106446

14. Wang C, Li KF, Hu XY, Yang HT, Zhou YJ (2021) Numerical study on laser shock peening of TC4 titanium alloy based on the plate and blade model. Opt Laser Technol 142:107163. https://doi.org/10.1016/j.optlastec.2021.107163

15. Wu JJ, Xu ZH, Qiao HC, Zhao JB, Huang Z (2021) Mechanical properties prediction of superalloy FGH4095 treated by laser shock processing based on machine learning. Mater Lett 297:129970. https://doi.org/10.1016/j.matlet.2021.129970

16. Davidson MJ, Balasubramanian K, Tagore GRN (2008) Surface roughness prediction of flow-formed AA6061 alloy by design of experiments. J Mater Process Technol 202:41–46. https://doi.org/10.1016/j.jmatprotec.2007.08.065

17. Bagudanch I, Vives-Mestres M, Sabater M, Garcia-Romeu ML (2017) Polymer incremental sheet forming process: temperature analysis using response surface methodology. Mater Manuf Processes 32:44–53. https://doi.org/10.1080/10426914.2016.1176191

18. Mostafanezhad H, Menghari HG, Esmaeili S, Shirkharkolaee EM (2018) Optimization of two-point incremental forming process of AA1050 through response surface methodology. Measurement 127:21–28. https://doi.org/10.1016/j.measurement.2018.04.042

19. Chen C, Zhao SD, Han XL, Cui MC, Fan SQ (2016) Optimization of a reshaping rivet to reduce the protrusion height and increase the strength of clinched joints. J Mater Process Technol 234:1–9. https://doi.org/10.1016/j.jmatprotec.2016.03.006

20. Eshtayeh M, Hrairi M (2016) Multi objective optimization of clinching joints quality using Grey-based Taguchi method. Int J Adv Manuf Technol 87:233–249. https://doi.org/10.1007/s00170-016-8471-1

21. Roux E, Bouchard PO (2013) Kriging metamodel global optimization of clinching joining processes accounting for ductile damage. J Mater Process Technol 213:1038–1047. https://doi.org/10.1016/j.jmatprotec.2013.01.018

22. Oudjene M, Ben-Ayed L, Delamézière A, Batoz JL (2009) Shape optimization of clinching tools using the response surface methodology with moving least-square approximation. J Mater Process Technol 209:289–296. https://doi.org/10.1016/j.jmatprotec.2008.02.030

23. Wang MH, Xiao GQ, Li Z, Wang JQ (2018) Shape optimization methodology of clinching tools based on Bezier curve. Int J Adv Manuf Technol 94:2267–2280. https://doi.org/10.1007/s00170-017-0987-5

24. Schwarz C, Kropp T, Kraus C, Drossel W (2020) Optimization of thick sheet clinching tools using principal component analysis. Int J Adv Manuf Technol 106:471–479. https://doi.org/10.1007/s00170-019-04512-5

25. Fabbro R, Fournier J, Ballard P, Devaux D, Virmont J (1990) Physical study of laser-produced plasma in confined geometry. J Appl Phys 68:775–784. https://doi.org/10.1063/1.346783

26. Zhang WW, Yao YL (2002) Microscale laser shock processing of metallic components. J Manuf Sci Eng 124:369–378. https://doi.org/10.1115/1.1445149

27. Wielage H, Vollertsen F (2011) Classification of laser shock forming within the field of high speed forming processes. J Mater Process Technol 211:953–957. https://doi.org/10.1016/j.jmatprotec.2010.07.012

28. Johnson GR, Cook WH (1983) A constitutive model and data for metals subjected to large strains, high strain rates and high temperatures, 7th International Symposium on Ballistics. Hague, Netherlands, pp 541–547

29. Zheng C, Sun S, Ji Z, Wang W, Liu J (2010) Numerical simulation and experimentation of micro scale laser bulge forming. Int J Mach Tools Manuf 50:1048–1056. https://doi.org/10.1016/j.ijmachtools.2010.08.012

30. Myers RH, Montgomery DC, Anderson-Cook CM (2016) Response surface methodology: process and product optimization using designed experiments, 4th edn. Wiley, New Jersey

31. Fenske H, Vollertsen F (2019) Laser shock punching: principle and influencing factors. Prod Eng 13:399–407. https://doi.org/10.1007/s11740-019-00886-3

32. Kumar SP, Elangovan S (2020) Optimization in single point incremental forming of Inconel 718 through response surface methodology. Trans Can Soc Mech Eng 44:148–160. https://doi.org/10.1139/tcsme-2019-0003

33. Zhou YJ, Lan FC, Huang XH, Chen JQ (2011) Multi-objective optimization of geometry of clinching tools for steel-aluminum blank sheets. Mater Sci Technol 19:86–93. https://doi.org/10.11951/j.issn.1005-0299.20110616

34. Kramer O (2017) Genetic algorithm essentials. Springer, Cham

35. Zhou G, Ma ZD, Li GY, Cheng AG, Duan LB, Zhao WZ (2016) Design optimization of a novel NPR crash box based on multi-objective genetic algorithm. Struct Multidisc Optim 54:673–684. https://doi.org/10.1007/s00158-016-1452-z